Materials Physics and Mechanics 47 (2021) 608-612 Received: September 29, 2021
Research article

A MODEL FOR ANNEALING-INDUCED HARDENING IN ULTRAFINE-GRAINED METALS

A.G. Sheinerman[1*], S.A. Krasnitckii[2,3]

[1]Institute of Problems of Mechanical Engineering, Russian Academy of Sciences, St. Petersburg 199178, Russia

[2]Peter the Great St. Petersburg Polytechnic University, St. Petersburg 195251, Russia

[3]ITMO University, Kronverkskiy pr. 49, St. Petersburg 197101, Russia

*e-mail: asheinerman@gmail.com

Abstract. We suggest a model, which describes the effect of grain boundary relaxation on the annealing-induced hardening in ultrafine-grained metals. Within the model, grain boundary relaxation during annealing is accompanied by a decrease in the number of grain boundary dislocation sources. The exhaustion of easily activated grain boundary dislocation sources results in the activation of harder grain boundary dislocation sources and/or repetitive action of the same dislocation sources. This gives rise to an increase in the strain hardening rate that can lead to an increase in the ultimate strength of ultrafine-grained solids. The results of the model agree with available experimental data.
Keywords: ultrafine-grained materials; hardening; annealing; grain boundaries

1. Introduction

The effect of the annealing-induced hardening (AIH) has been observed in many nanocrystalline (NC) and ultrafine-grained (UFG) metals and alloys (see, e.g., review [1] and original works [2-12]). This effect is in contrast to the annealing-induced softening of coarse-grained metals and alloys associated with a decrease in the dislocation density and grain growth during annealing [1]. AIH in NC and UFG metals and alloys was attributed to various factors [1], among which one can distinguish annihilation of mobile dislocations, grain boundary (GB) sliding, GB relaxation (that is, a decrease in the GB specific energies and defect density at GBs), arrangement of dislocations into dislocation walls, solute segregations at GBs, dislocations or twin boundaries, formation of stacking faults and twinning. In particular, AIH of a UFG Ni alloy [10] and Ti [2] was accompanied by the observed dislocation clustering into low-angle GBs [2,10]. In contrast, in UFG Cu-Al-Zn alloys, AIH was shown to result from the solute segregation to lattice defects, twinning, and the formation of stacking faults during annealing [7,8]. In NC alloys and UFG Zn-based alloys, where plastic deformation can be realized via GB sliding at room temperature, annealing was demonstrated to hinder GB sliding, probably, as a result of GB relaxation and GB solute segregation, resulting in AIH [4,6,9].

Orlova et al. [11] suggested a model describing AIH in UFG Al documented in this work for the situation where plastic deformation in UFG Al involves limited GB sliding accommodated by GB dislocation climb and lattice dislocation motion from one GB to another. The presence of limited GB sliding in UFG Al at room temperature [11] was indirectly confirmed in ref. [12], which demonstrated a strong temperature dependence of the AIH effect that correlated well with the temperature dependence of GB sliding. At the same time, GB sliding is not commonly observed in UFG metals at room temperature, and such

http://dx.doi.org/10.18149/MPM.4742021_8

metals are often believed to primarily deform via the emission of lattice dislocations from GBs [13]. In this case, annealing-induced GB relaxation can decrease the number of GB sources for lattice dislocation emission. This can lead to the dislocation source exhaustion and the resulting AIH. The aim of the present paper is to suggest a model that describes the effect of the GB dislocation source exhaustion on AIH in UFG metals and alloys.

2. Theory

Consider a UFG metallic solid under the action of a uniaxial tensile load (Fig. 1). We assume that plastic deformation in this solid occurs by dislocation emission from GB dislocation sources, their motion across grains, and absorption by GBs. We denote the average distance between adjacent GB sources in GBs as p and the magnitude of the dislocation Burgers vector as b. The dislocations at GBs can induce significant back stresses, resulting in strain hardening.

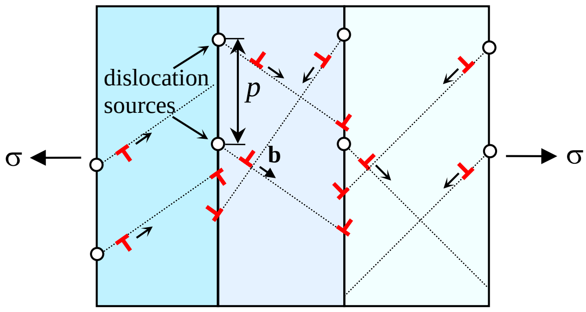

Fig. 1. A fragment of a UFG metallic solid under tensile load σ. Dislocations are generated at GB dislocation sources and move across grains to adjacent GBs

At the same time, the buildup of the local stresses at GBs leads to the relaxation processes via the motion and annihilation of GB dislocations. This situation can be described by the model of Proudhon et al. [14]. Within this approach, the average number $\bar{N}$ of dislocations that can be stored at GBs (per GB dislocation source) can be related to the plastic strain ε_p via an empirical expression that leads to the saturation of the number of dislocations in GBs [15]:

$$\frac{\partial \bar{N}}{\partial \varepsilon_p} = \frac{Mp}{b}\left(1 - \frac{\bar{N}}{n^* p}\right). \tag{1}$$

In formula (1) n^* is the fitting parameter that has the meaning of the maximum number of dislocations per unit GB length that can be stored at a GB, and M is the Taylor factor (equal to 3.06 for isotropic face-centered cubic metallic matrices [16]). The first term in formula (1) describes an increase $\bar{N}^+$ in the number of dislocations due to dislocation emission from GB dislocation sources, which is calculated as $\bar{N}^+ = (Mp/b)\varepsilon_p$. The second term in this formula describes dislocation annihilation at GBs. The solution of Eq. (1) for ε_p has the form

$$\varepsilon_p = -\frac{bn^*}{M}\ln\left(1 - \frac{\bar{N}}{n^* p}\right). \tag{2}$$

Consider a specified dislocation source in a GB. Let σ_0 be the critical applied load for the emission of the first dislocation from this GB dislocation source (hereafter referred to as the source strength), and N be the number of dislocations stored at an opposite GB due to the action of this dislocation source. (This number is equal to the number of dislocations emitted from this dislocation source and not annihilated at the opposite GB.) To calculate the critical applied load σ for dislocation emission from the GB dislocation source, we follow refs. [17,18] that supposed the existence of linear dependence between the flow stress and the number of dislocations stored at GBs. Similarly, we assume that the critical applied load σ linearly depends on the number N' of dislocations previously stored at the GB due to the action of the specified dislocation source. Under this assumption, the critical applied load σ can be written as $\sigma = \sigma_0 + \alpha G N'$, where G is the shear modulus, and α is a numerical factor. This means that the number N' of dislocations stored at the GB due to the action of the dislocation source prior to the emission of a new dislocation follows as $N' = (\sigma - \sigma_0)/(\alpha G)$ for $\sigma \geq \sigma_0$. Also, when a new dislocation is emitted from the GB source, it is stored at the opposite GB (that is, not annihilated) with the probability equal to $\bar{N}^+/\bar{N}$. Thus, the average number N of dislocations stored at a GB due to the action of a dislocation source with the strength σ_0 is given by

$$N = [\bar{N}^+/\bar{N} + (\sigma - \sigma_0)/(\alpha G)]H(\sigma - \sigma_0), \tag{3}$$

where $H(x)$ is the Heaviside function equal to unity for $x > 0$, and to zero otherwise.

To account for the effect of the source strength distribution, now assume that the dislocation source strength obeys the lognormal distribution with the mean source strength $\bar{\sigma}_0$, described by the probability density

$$\rho(\sigma_0) = \frac{1}{\sigma_0\sqrt{2\pi s^2}} \exp\left[-\frac{(\ln(\sigma_0/\bar{\sigma}_0) + s^2/2)^2}{2s^2}\right], \tag{4}$$

where s denotes the dispersion of $\ln\sigma_0$. Then the average number $\bar{N}$ of dislocations that can be stored at a GB (per GB dislocation source) can be calculated as $\bar{N} = \int_0^\infty N\rho(\sigma_0)\,d\sigma_0$. Substituting formula (3) to the latter relation, one obtains:

$$\bar{N} = (\bar{N}/\bar{N}^+) f_1(\sigma) + f_2(\sigma), \tag{5}$$

where $f_1(\sigma) = \int_0^\sigma \rho(\sigma_0)\,d\sigma_0$ and $f_2(\sigma) = [1/(\alpha G)]\int_0^\sigma \rho(\sigma_0)(\sigma - \sigma_0)\,d\sigma_0$. Substitution of equality $\bar{N}^+ = (Mp/b)\varepsilon_p$ and formula (2) into (5) provides the following equation for $\bar{N}$:

$$\bar{N}\left(1 + \frac{f_1(\sigma)}{n^* p \ln[1 - \bar{N}/(n^* p)]}\right) = f_2(\sigma). \tag{6}$$

Solving equation (6) for $\bar{N}$ and using formula (2), one can relate the plastic strain ε_p to the true flow stress σ. Also, the total true strain ε can be calculated as $\varepsilon = \sigma/E + \varepsilon_p$, where E is the Young modulus of the specimen.

3. Results

Using the above equation, we calculate the dependences of the true flow stress σ on true strain ε for the case of UFG Al characterized by the following values of parameters: $G = 27$ GPa, $E = 70$ GPa, $b = 0.286$ nm. We also put $s = 0.25$, $\bar{\sigma}_0 = 290$ MPa and $\alpha = 0.007$. Figure 2a plots the dependences $\sigma(\varepsilon)$ for the UFG Al specimen with $n^* = 0.06$ nm^{-1} and two different values of the GB dislocation source spacing: $p = 15$ nm (solid blue line) and 25 nm (solid red line).

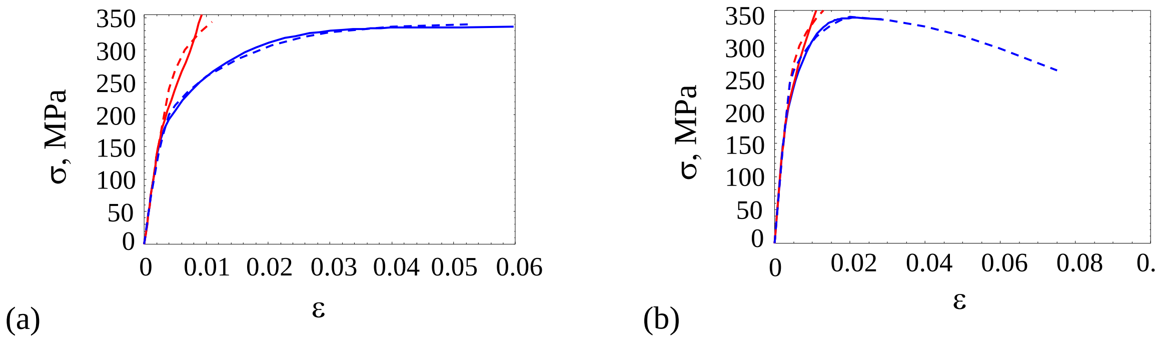

Fig. 2. Calculated (solid lines) and experimental (dashed lines) tensile stress-strain curves for UFG Al. The experimental dashed curves are taken from ref. [5] (a) and ref. [3] (b)

The dashed curves depict the experimental tensile true stress–true strain curves [5] for UFG commercial purity Al before (dashed blue curve) and after (dashed red curve) annealing at 175°C for one hour. It is seen that the calculated curves agree well with the experimental ones. The calculated curves also demonstrate that a decrease in the number of GB dislocation sources due to the low-temperature annealing (which manifests itself in the increase in the GB source spacing from 15 to 25 nm) results in a strong increase in the work-hardening rate, and, as a consequence, in a rise of the flow stress at a specified strain.

Using the relations $\varepsilon_e = e^{\varepsilon} - 1$ and $\sigma_e = \sigma/(1+\varepsilon)$, one can relate the true flow stress σ and true strain ε to the engineering flow stress σ_e and engineering strain ε_e. Figure 2b displays the calculated engineering stress–engineering strain curves for UFG Al with $n^* = 0.015$ nm^{-1}, $p = 30$ nm (solid blue line) and 38 nm (solid red line). The dashed curves illustrate the experimental tensile engineering stress–engineering strain curves [3] for UFG commercial purity Al before (dashed blue curve) and after (dashed red curve) annealing at 150°C for 30 min. The calculated curves in Fig. 2b match the experimental ones, at least, until the onset of necking instability characterized by the maximum at the blue curves. Figure 2b shows that a decrease in the number of GB dislocation sources owing to the low-temperature annealing leads to an increase in both the work-hardening rate and the ultimate strength, although at the expense of reduced ductility.

4. Concluding remarks

In summary, GB relaxation via low-temperature annealing, which manifests itself in a decrease in the number of GB dislocation sources, seems to reasonably explain AIH in UFG metals. Within our model, the controlling parameter that determines the character of the stress-strain dependence, as well as the ultimate strength and ductility of UFG metallic solids is the distance p between GB dislocation sources. A decrease in the number of GB dislocation sources leads to the dislocation source exhaustion. The activation of new GB dislocation sources with higher activation stress or the repeated activation of the same GB dislocation source requires a load increase. This gives rise to the observed (e.g., [1,3,5]) increase in the strain hardening rate that can lead to an increase in the ultimate strength of UFG solids.

Acknowledgements. *The work is supported by the Russian Ministry of Science and Higher Education within the World-Class Research Center Program "Advanced Digital Technologies" (contract 075-15-2020-934 of 17.11.2020).*

References

[1] Gubicza J. Annealing-induced hardening in ultrafine-grained and nanocrystalline materials. *Advanced Engineering Materials.* 2020;22(1): 1900507.
[2] Valiev RZ, Sergueeva AV, Mukherjee AK. The effect of annealing on tensile deformation behavior of nanostructured SPD titanium. *Scripta Materialia*. 2003;49(7): 669-674.
[3] Huang X, Hansen N, Tsuji N. Hardening by annealing and softening by deformation in nanostructured metals. *Science*. 2006;312(5771): 249-251.
[4] Detor AJ, Schuh CA. Microstructural evolution during the heat treatment of nanocrystalline alloys. *Journal of Materials Research.* 2007;22(1): 3233-3248.
[5] Bowen JR. Strength and structure in commercial purity aluminium after large strain. *Materials Science and Engineering A.* 2008;483-484: 231-234.
[6] Yang CF, Pan JH, Lee TH. Work-softening and anneal-hardening behaviors in fine-grained Zn–Al alloys. *Journal of Alloys and Compounds.* 2009;468(1-2): 230-236.
[7] Zhou S, Lv W, Li P, Gong Y, Tao J, Cheng L, Zhu X. Mechanical properties and deformation kinetics of bulk Cu–Al–Zn alloy subjected to rolling and annealing. *Materials Science and Engineering A.* 2014;609: 217-221.
[8] Gong YL, Ren SY, Zeng SD, Zhu XK. Unusual hardening behaviour in heavily cryo-rolled Cu-Al-Zn alloys during annealing treatment. *Materials Science and Engineering A.* 2016;659: 165-171.
[9] Hu J, Shi YN, Sauvage X, Sha G, Lu K. Grain boundary stability governs hardening and softening in extremely fine nanograined metals. *Science*. 2017;355(6331): 1292-1296.
[10] Gubicza J, Pereira PHR, Kapoor G, Huang Y, Subramanya Sarma V, Langdon TG. Annealing-induced hardening in ultrafine-grained Ni–Mo alloys. *Advanced Engineering Materials*. 2018;20(9): 1800184.
[11] Orlova TS, Skiba NV, Mavlyutov AM, Murashkin MY, Valiev RZ, Gutkin MY. Hardening by annealing and implementation of high ductility of ultra-fine grained aluminum: experiment and theory. *Reviews on Advanced Materials Science*. 2018;57(2): 224-240.
[12] Orlova TS, Mavlyutov AM, Gutkin MY. Suppression of the annealing-induced hardening effect in ultrafine-grained Al at low temperatures. *Materials Science and Engineering A*. 2021;802: 140588.
[13] Ovid'ko IA, Valiev RZ, Zhu YT. Review on superior strength and enhanced ductility of metallic nanomaterials. *Progress in Materials Science*. 2018;94: 462-540.
[14] Proudhon H, Poole WJ, Wang X, Brechet Y. The role of internal stresses on the plastic deformation of the Al-Mg-Si-Cu alloy AA6111. *Philosophical Magazine*. 2008;88(5): 621-640.
[15] Xu R, Tan Z, Fan G, Ji G, Li Zan, Guo Q, Li Zhiqiang, Zhang D. Microstructure-based modeling on structure-mechanical property relationships in carbon nanotube/aluminum composites. *International Journal of Plasticity*. 2019;120: 278-295.
[16] Taylor GI. Plastic strain in metals. *Journal of the Institute of Metals*. 1938;62: 307-324.
[17] Delince M, Brechet Y, Embury JD, Geers MJD, Jacques PJ, Pardoen T. Structure-property optimization of ultrafine-grained dual-phase steels using a micro structure-based strain hardening model. *Acta Materialia*. 2007;55(7): 2337-2350.
[18] Zhu LL, Lu J. Modelling the plastic deformation of nanostructured metals with bimodal grain size distribution. *International Journal of Plasticity.* 2012;30-31: 166-184.